Theory of two-dimensional grating couplers

Lian Zheng, W. L. Schaich, and A. H. MacDonald
Department of Physics and Materials Research Institute, Indiana University, Bloomington, Indiana 47405
(Received 4 December 1989)

We derive and evaluate expressions for the electromagnetic coupling between a two-dimensional grating and a nearby two-dimensional electron gas. By considering both the thickness and the separation of the two systems as small compared with macroscopic wavelengths, a numerically tractable prescription for their mutual influence on an incident beam is developed. The theory is evaluated in several model calculations, which compare favorably with recent far-infrared transmission studies of cyclotron and magnetoplasmon resonances. The general need for a nonperturbative analysis is illustrated.

I. INTRODUCTION

A common way to study the excitations of electron systems with reduced dimensionality is with infrared absorption.[1-3] In order to increase the range of wave vectors that can be so examined, one often uses a planar grating coupler of period a to allow jumps in the probe wave vector parallel to the plane by

$$G_n=(2\pi/a)n \ , \tag{1}$$

where n is an integer.[4,5] A schematic of the experimental arrangement is shown in Fig. 1. Typically, light is incident along the surface normal and one measures the net transmission T. Since the physical thickness of such a grating is often much smaller than its separation d from the similarly confined electron system, the optical problem may be idealized to the coupled response of a pair of two-dimensional layers. Further, because a is much smaller than the wavelength of light in either of the surrounding media, any field with a parallel variation set by G_n with $n\neq 0$ cannot propagate away; i.e., all of the diffracted beams are evanescent. The task of theory is then to describe consistently these local fields near the interface and their influence on the transmission of the zeroth-order beam.

In this paper we begin an analysis of how one can theoretically formulate and evaluate the effect of the grating coupler. For simplicity we treat the confined electron system as a homogeneous, two-dimensional, free-electron gas (called henceforth the 2D-EG), whose electrical response is characterized by an areal density N, an effective mass m^*, and a Drude relaxation time τ. We postpone to later work the study of more complicated features in the 2D-EG since our present emphasis is on the influence of the grating. The first papers that employed such experimental methods outline a perturbative scheme for treating the grating's influence.[4-8] The derivation that we developed in Sec. II is more complete and more general. We do confirm the earlier perturbative expressions, but also can calculate in regimes where they fail. This always occurs as τ is increased, so the continuing improvements in 2D-EG sample quality mandate such improvements in the theory.

Our theory also can explain a novel experimental feature that appears in comparing cyclotron resonance signals observed without and with a grating coupler.[9] When there is no grating present, the maximum change in the transmission of an unpolarized incident beam is 50%. This is easy to understand if one considers the incident light to have equal amounts of right and left circularly polarized light. The cyclotron absorption on resonance blocks one of these, but leaves the other essentially unaffected. The puzzle is that when one adds a grating coupler, the maximum charge in transmission increases to well over 50%.[9]

This effect, however, is also simple to rationalize once one acknowledges the polarizing action of the grating. Let $\hat{\mathbf{z}}$ be the direction along the metal strips of the grat-

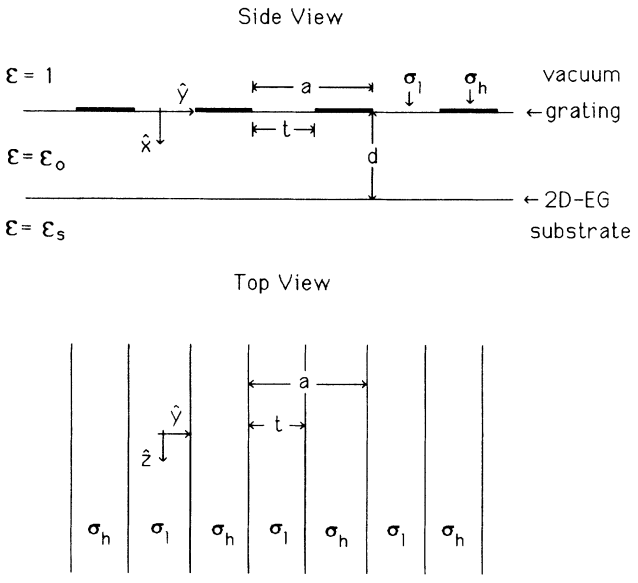

FIG. 1. Qualitative sketch of the interface region showing how various parameters in the text are defined. Both side and top views are given. The spatial variation of the grating conductivity is here imagined to be due to thin metal strips along $\hat{\mathbf{z}}$, of different thickness along $\hat{\mathbf{x}}$.

ing and $\hat{\mathbf{y}}$ be the orthogonal direction in the grating plane, see Fig. 1. For simplicity characterize the (diagonal but anisotropic) conductivity of the grating by the (artificial) homogeneous values of infinity along $\hat{\mathbf{z}}$ and zero along $\hat{\mathbf{y}}$. This makes an isolated grating a simple linear polarizer. There can be no electric field along $\hat{\mathbf{z}}$ in its near vicinity. Hence there is no significant electric field along $\hat{\mathbf{z}}$ in the 2D-EG as long as the separation d in Fig. 1 is much less than the wavelength. In the presence of a static magnetic field along $\hat{\mathbf{x}}$, the surface normal, the incident radiation will cause current to flow in the 2D-EG along both the $\hat{\mathbf{y}}$ and $\hat{\mathbf{z}}$ axes, but that along $\hat{\mathbf{z}}$ will be effectively canceled by an image current in the grating. Hence only the σ_{yy} component of the 2D-EG conductivity can influence the transmission coefficient, independent of whether there is or is not an applied static magnetic field present. For an unpolarized incident beam, the transmission coefficient is then easily shown to be

$$T=\tfrac{1}{2}T_y=\tfrac{1}{2}(\epsilon_s)^{1/2}\left|\frac{2}{1+(\epsilon_s)^{1/2}+\frac{4\pi}{c}\sigma_{yy}}\right|^2, \tag{2}$$

where c is the speed of light and ϵ_s is the dielectric constant of the substrate. At the cyclotron resonance σ_{yy} becomes large and the drop in T can exceed 50%.

We will numerically demonstrate this behavior in Sec. III along with the predictions of a more realistic analysis. We also will present model calculations of the signal strength predicted for the magnetoplasmon resonances which occur at larger wave vectors. The dependence of these and of the cyclotron resonance on the parameters of the grating and of the 2D-EG will be illustrated and comparisons made with more approximate estimates of the grating coupler efficiency.

II. FORMALISM

The physical assumptions about the system geometry allow several important simplifications in the analysis. If the zeroth-order beam is moving along the surface normal, only the induced currents lying in and averaged over the surface plane can influence the reflection and transmission amplitudes. One can then separate the problem into two stages: first to calculate the microscopic surface currents for different choices of perturbing fields and second to determine their effect on the zeroth-order beam.

We begin with the latter task since it is the easier of the two. One is looking for the modifications to the Fresnel reflection and transmission coefficients, when light from vacuum strikes at normal incidence a dielectric whose bulk response is characterized by ϵ_s and which in addition can generate surface localized currents described by the constitutive relation

$$\langle \underline{J} \rangle = \underline{\underline{\Sigma}} \cdot \underline{E}^0 , \tag{3}$$

where both the surface current density $\langle \underline{J} \rangle$ and the electric field $\underline{E}^0$ lie in the surface plane, and neither depends on position in this plane. We are postponing until later in this section the calculation of the 2×2 tensor $\underline{\underline{\Sigma}}$, which describes the net effect of the microscopic structure of two conducting layers; i.e., of grating coupler plus 2D-EG. The surface currents in (3) lead to the following boundary conditions for macroscopic fields moving along the surface normal:

$$\Delta \underline{E}^0 = \underline{0} , \tag{4a}$$

$$\hat{\mathbf{x}} \times \Delta \underline{B}^0 = \frac{4\pi}{c}\langle \underline{J} \rangle , \tag{4b}$$

where Δ denotes "the jump in value across the interface of."

It is now straightforward to solve for the macroscopic fields. One writes down linear combinations of partial waves that satisfy Maxwell's equations away from $x=0$ and which represent the incident, reflected, and transmitted beams. The unknown amplitudes of these partial waves are determined by requiring Eq. (4) to hold. We will illustrate the procedure for an incident beam polarized along $\hat{\mathbf{y}}$. The electric field is written as

$$\vec{E}^{\,0} = e^{-i\omega t}\begin{cases}(0,1,0)e^{ipx}+(0,E_y^r,E_z^r)e^{-ipx}, & x<0\\ (0,E_y^t,E_z^t)e^{ip'x}, & x>0\end{cases} \tag{5}$$

where $p=\omega/c$ and $p'=\omega(\epsilon_s)^{1/2}/c$, with ω the light frequency. The triplets of numbers describe the Cartesian components of the partial waves along $\hat{\mathbf{x}}$, $\hat{\mathbf{y}}$, and $\hat{\mathbf{z}}$. From Faraday's law the corresponding magnetic field is

$$\vec{B}^{\,0} = e^{-i\omega t}\begin{cases}(0,0,1)e^{ipx}+(0,E_z^r,-E_y^r)e^{-ipx}, & x<0\\ (\epsilon_s)^{1/2}(0,-E_z^t,E_y^t)e^{ip'x}, & x>0\end{cases} \tag{6}$$

wherein the same four unknown amplitudes appear. These are found by invoking (4) and using (3) with $\underline{E}^0$ there evaluated at $x=0$.

We skip the intermediate algebraic steps to write the results for the transmission coefficient as

$$T_y=(\epsilon_s)^{1/2}(|E_y^t|^2+|E_z^t|^2) , \tag{7}$$

where

$$E_z^t=\left[-\frac{4\pi}{c}\Sigma_{zy}\right]E_y^t\Big/\left[1+(\epsilon_s)^{1/2}+\frac{4\pi}{c}\Sigma_{zz}\right] \tag{8}$$

and

$$E_y^t=2\Big/\left[1+(\epsilon_s)^{1/2}+\frac{4\pi}{c}\Sigma_{yy}-\frac{\left[\frac{4\pi}{c}\Sigma_{yz}\right]\left[\frac{4\pi}{c}\Sigma_{zy}\right]}{1+(\epsilon_s)^{1/2}+\frac{4\pi}{c}\Sigma_{zz}}\right] . \tag{9}$$

The answer for an incident beam polarized along $\hat{\mathbf{z}}$ may be written as in (7)–(9) but with every y subscript changed to a z subscript and vice versa. For an unpolarized incident beam one should use

$$T=\tfrac{1}{2}(T_y+T_z) . \tag{10}$$

Note that elements of the two-dimensional conductivity

$\underset{\sim}{\Sigma}$ may be considered as large or small depending on whether they are greater or less than

$$\frac{c}{4\pi}=1/(377\ \Omega)\ . \tag{11}$$

The "perfect polarizer" limit discussed in the Introduction can be extracted from these equations by letting $\Sigma_{zz}\to\infty$ and replacing all other Σ elements with the corresponding elements of the 2D-EG conductivity. As we show in Sec. III, this can be adequate for describing cyclotron resonance signals, but it completely misses magnetoplasmon effects. Hence we turn to more sophisticated estimates of $\underset{\sim}{\Sigma}$.

Again the small thickness and period of the grating and its small separation from the 2D-EG allow us to simplify the equations. In contrast to the above calculations where the spatial variation of the transverse electromagnetic fields is evident while the longitudinal fields are hidden in the constitutive relation for the averaged surface current $\langle \underset{\sim}{J} \rangle$, we now want to examine the longitudinal fields in detail which means that we will be working on a spatial scale where the transverse fields can be treated as constant. Further we assume that the grating inhomogeneity depends only on y in the surface plane and that it is not only periodic in y but also an even function of y. This allows us to expand the surface currents in a cosine Fourier series in y and sets the parity of the various microscopic field components.

We shall neglect the finite thickness of both the grating and the 2D-EG, treating each as a strictly two-dimensional layer. This excludes (for now) a treatment of intersubband transitions, which have been observed both without and with grating couplers—see the examples in Ref. 3. It also prevents a discussion of grating couplers with non-negligible thickness; e.g., those based on deep grooves of dielectric rather than just thin layers of metal.[10–13] A more involved grating theory is necessary for these.[14]

The in-plane response of the grating and the 2D-EG are treated quite differently. We assume the grating conductivity is diagonal and local, but due to its inhomogeneity has a macroscopic anisotropy. The current is written as

$$\underset{\sim}{J}^{(g)}(y)=\sum_{n\geq 0}\underset{\sim}{J}^{(g)}(n)\cos(G_n y) \tag{12a}$$

$$=\underset{\sim}{\sigma}^{(g)}(y)\cdot\underset{\sim}{E}^{(g)}(y) \tag{12b}$$

where the superscript g denotes grating. The precise functional dependence of the conductivity tensor on y is not crucial; we only require that it can be expanded as

$$\underset{\sim}{\sigma}^{(g)}(y)=\sum_{n\geq 0}\underset{\sim}{\sigma}^{(g)}(n)\cos(G_n y)\ . \tag{13}$$

A similar expansion holds for the grating's resistivity tensor

$$\underset{\sim}{\rho}^{(g)}(y)=[\underset{\sim}{\sigma}^{(g)}(y)]^{-1}=\sum_{n\geq 0}\underset{\sim}{\rho}^{(g)}(n)\cos(G_n y)\ . \tag{14}$$

For the 2D-EG we allow its conductivity to be nondiagonal and nonlocal, but presume it (for now) to be isotropic and homogeneous. The latter two constraints can be removed without greatly complicating the formal theory, but we postpone this extension to a future paper.[15] The 2D-EG current is written in cosine Fourier space as

$$\underset{\sim}{J}(n)=\underset{\sim}{\sigma}(n)\cdot\underset{\sim}{E}(n)\ , \tag{15}$$

in which the parallel electric field is that at the plane of the 2D-EG. Our model calculations in Sec. III ignore the n dependence of $\underset{\sim}{\sigma}(n)$, which suppresses in particular the excitation of cyclotron resonance harmonics.[11,16,17] It can be easily restored.

To get a closed set of equations for the currents in (12) and (15) we need to describe the electric field near the interface. We separate the total field $\vec{E}$ into

$$\vec{E}(\vec{x})=\vec{E}_T+\vec{E}_L(\vec{x})\ , \tag{16}$$

where

$$\vec{E}_T=(0,e_y,e_z) \tag{17}$$

is constant and represents the slowly varying transverse fields near the interface. Comparing for example with (5) we would identify $e_y=E_y^t=1+E_y^r$ and $e_z=E_z^t=E_z^r$. The strong microscopic variation of $\vec{E}$ lies in the longitudinal field $\vec{E}_L(\vec{x})$ which we expand as

$$\vec{E}_L(\vec{x})=\begin{cases}\displaystyle\sum_{n>0} r_n\,(\sin(G_n y),\cos(G_n y),0)\,e^{G_n x}, & x<0\\ \displaystyle\sum_{n>0}[\lambda_n^{(-)}(-\sin(G_n y),\cos(G_n y),0)\,e^{-G_n x}+\lambda_n^{(+)}(\sin(G_n y),\cos(G_n y),0)\,e^{G_n(x-d)}], & 0<x<d\\ \displaystyle\sum_{n>0} t_n\,(-\sin(G_n y),\cos(G_n y),0)\,e^{-G_n(x-d)}, & d<x\end{cases} \tag{18}$$

where $x=0$ is the location of the grating and $x=d$ that of the 2D-EG. Away from these planes $\vec{E}_L$ has zero divergence and zero curl. Consistent with our neglect of spatial variation in the transverse fields, the speed of light does not enter the wave vectors in (18); i.e., $\vec{E}_L$ is the electrostatic approximation to the longitudinal field generated by the charge accumulations in the pair of two-dimensional layers. We are also neglecting spatially varying transverse electric (or magnetic) fields, which is a standard approximation in problems of local field

effects,[18] since their relative contribution is reduced by factors of $\omega/G_n c \ll 1$.

The parameters in (18) are to be determined by the boundary conditions across each layer:

$$\Delta E_y = 0 , \tag{19a}$$

$$\Delta D_x = \frac{4\pi}{i\omega}(\underline{\nabla}\cdot\underline{J}) , \tag{19b}$$

where we have introduced the displacement field $\vec{D}=\epsilon(x)\vec{E}$ with

$$\epsilon(x)=\begin{cases} 1, & x<0 \\ \epsilon_0, & 0<x<d \\ \epsilon_s, & d<x \end{cases} \tag{20}$$

and have used the equation of continuity in each layer to express the induced charge density in terms of a divergence of the microscopic current. For the 2D-EG this divergence may be simply expressed as

$$\underline{\nabla}\cdot\underline{J} = -\sum_{n>0} G_n \sigma_{yy}(n) t_n \sin(G_n y) , \tag{21}$$

while for the grating it depends on the functional form of $\underset{\sim}{\sigma}^{(g)}(y)$.

Substituting $\vec{E}_L$ of (18) into (19) and using (21) we can eliminate $\lambda_n^{(+)}$, $\lambda_n^{(-)}$, and t_n from the resulting set of four equations for each $n\neq 0$ to arrive at

$$r_n F_n = J_y^{(g)}(n) \tag{22}$$

where

$$F_n = \frac{i\omega}{4\pi G_n}\left[1+\epsilon_0 \coth(G_n d) + \frac{\epsilon_0^2[1-\coth^2(G_n d)]}{\frac{4\pi i}{\omega} G_n \sigma_{yy}(n) + \epsilon_s + \epsilon_0 \coth(G_n d)} \right] . \tag{23}$$

Only y components appear in (22) and (23) because there are no fluctuating fields along $\hat{\mathbf{z}}$ nor does any quantity vary with z.

Before trying to solve (22) recall that we seek

$$\langle \underline{J} \rangle = \underset{\sim}{\sigma}(n=0)\cdot\underline{E}_T + \underline{J}^{(g)}(n=0) \tag{24}$$

where

$$J_z^{(g)}(n=0) = \left[\frac{1}{a}\int_0^a dy\, \sigma_{zz}^{(g)}(y)\right] e_z \equiv \bar{\sigma} e_z \tag{25}$$

is easily calculated and $\underset{\sim}{\sigma}(n=0)$ is known. Hence the only unknown is from (12) and (18)

$$J_y^{(g)}(n=0) \equiv j_0 = \left[\frac{1}{a}\int_0^a dy\, \sigma_{yy}^{(g)}(y)\right] e_y + \tfrac{1}{2}\sum_{k>0} \sigma_{yy}^{(g)}(k) r_k , \tag{26}$$

which in this form requires the r_k. To determine these one could formally use (12) to find for $n\neq 0$

$$J_y^{(g)}(n) = \sigma_{yy}^{(g)}(n) e_y + \left[\frac{1}{a}\int_0^a dy\, \sigma_{yy}^{(g)}(y)\right] r_n + \tfrac{1}{2}{\sum_{m>0}}' \sigma_{yy}^{(g)}(m)(r_{n+m}+r_{|n-m|}) . \tag{27}$$

The prime on the summation is a reminder that the term with $r_{k=0}$ should be excluded. The combination of Eq. (27) with Eq. (22) should allow one to eliminate the $J_y^{(g)}(n)$ and solve for the r_n as proportional to e_y.

We shall actually follow an alternate route based on a suggestion of Theis,[19] which uses resistivity tensors to eliminate the r_n so one can solve for the $J_y^{(g)}(n)$ as proportional to j_0. This approach starts from the inverse of (12b)

$$\underline{E}^{(g)}(y) = \underset{\sim}{\rho}^{(g)}(y)\cdot\underline{J}^{(g)}(y) \tag{12'}$$

which implies an inverse analog of (26)

$$E_y^{(g)}(n=0) \equiv e_y = \left[\frac{1}{a}\int_0^a dy\, \rho_{yy}^{(g)}(y)\right] j_0 + \tfrac{1}{2}\sum_{k>0} \rho_{yy}^{(g)}(k) J_y^{(g)}(k) . \tag{28}$$

To simplify the notation define

$$\bar{\rho} = \frac{1}{a}\int_0^a dy\, \rho_{yy}^{(g)}(y) , \tag{29}$$

$$\tilde{\rho}(k) = \rho_{yy}^{(g)}(k) , \tag{30}$$

$$\tilde{j}(k) = J_y^{(g)}(k)/j_0 \quad \text{for } k>0 . \tag{31}$$

Then (28) becomes

$$j_0/e_y = \left[\bar{\rho} + \tfrac{1}{2}\sum_{k>0} \tilde{\rho}(k)\tilde{j}(k)\right]^{-1} , \tag{32}$$

which requires the $\tilde{j}(k)$ to determine j_0. To find these we use (12') to find for $n\neq 0$

$$r_n = \left[\bar{\rho}\tilde{j}(n) + \tilde{\rho}(n) + \tfrac{1}{2}{\sum_{m>0}}' \tilde{\rho}(m)[\tilde{j}(n+m)+\tilde{j}(|n-m|)]\right] j_0 \tag{33}$$

where again the sum excludes the term with $\tilde{j}(k=0)$. Substituting (33) into (22) formally eliminates the r_n:

$$\tilde{j}(n)/F_n = \bar{\rho}\tilde{j}(n) + \tilde{\rho}(n) + \tfrac{1}{2}{\sum_{m>0}}' \tilde{\rho}(m)[\tilde{j}(n+m)+\tilde{j}(|n-m|)] . \tag{34}$$

After solving (34) for the $\tilde{j}(n)$, one uses (32) to find the proportionality between j_0 and e_y which finally allows the determination of $\underset{\sim}{\Sigma}$ from (24)–(26) as

$$\underset{\sim}{\Sigma} = \underset{\sim}{\sigma}(n=0) + \begin{bmatrix} j_0/e_y & 0 \\ 0 & \bar{\sigma} \end{bmatrix} . \tag{35}$$

The "perfect polarizer" approximation of the Introduction sets j_0/e_y to zero and $\bar{\sigma}$ to infinity.

To numerically implement either of the two solution schemes outlined above, which are formally equivalent, requires a truncation of a Fourier series so that matrices of finite dimension may be used. We have found that our results can be unphysically sensitive to the choice of this cutoff if we use conductivities and try to truncate the r_n series, while no such difficulty appears if we use resistivities and truncate the $\tilde{j}(n)$ series.[20] The physics behind this distinct numerical behavior is that there are strong spatial fluctuations in the electric field at the grating, but relatively weak variations in the microscopic current density. Hence one can be more successful in approximating high Fourier coefficients in $J_y^{(g)}$ than in $E_y^{(g)}$.

Before turning to model calculations, we make note of a perturbative estimate of j_0/e_y. If we assume that $F_n\bar{\rho}$ and $F_n\tilde{\rho}(m)$ are all much smaller than unity, then we can extract from (34) the analytic estimate

$$\tilde{j}(n)\approx\tilde{\rho}(n)F_n \ , \tag{36}$$

which when substituted into (32) and expanded again yields

$$j_0/e_y\approx 1/\bar{\rho}-\tfrac{1}{2}\sum_{k>0}\left[\frac{\tilde{\rho}(k)}{\bar{\rho}}\right]^2 F_k \ . \tag{37}$$

This result, used in (35) to determine Σ, which in turn determines T in (10), is equivalent to the perturbative estimates found by others. Its validity depends on none of the F_n becoming large, which fails when τ increases so one can be near a zero of the denominator in (23).

III. MODEL CALCULATIONS

In this section we give some numerical illustrations of our formal results. The models chosen are rather simple but still can reasonably represent a wide range of experimental configurations.

We begin with the grating taken in isolation, i.e., the 2D-EG is removed and one has only a substrate with $\epsilon_s=12.8$ in $x>0$. The conductivity is assumed to have a step profile, with $\sigma_l=1/\rho_h$ over a width t and $\sigma_h=1/\rho_l$ over the remainder of the period, $a-t$, see Fig. 1. The high and low values of conductivity as well as the ratio of t/a will be varied to exhibit trends. Our simple choice for the conductivity profile yields immediately

$$\bar{\sigma}=\frac{t}{a}\sigma_l+\left[1-\frac{t}{a}\right]\sigma_h \ , \tag{38}$$

$$\bar{\rho}=\frac{t}{a}\rho_h+\left[1-\frac{t}{a}\right]\rho_l \ , \tag{39}$$

$$\tilde{\rho}(k\neq 0)=\frac{2}{\pi k}(\rho_h-\rho_l)\sin(\pi kt/a) \ , \tag{40}$$

and in the absence of the 2D-EG

$$F_n=\frac{i\omega}{4\pi G_n}(1+\epsilon_s)=i\left[\frac{\nu a}{n}\right](1+\epsilon_s)\left[\frac{c}{4\pi}\right] \ , \tag{41}$$

where $\nu=\omega/(2\pi c)$ is the light frequency expressed in wave numbers. A basic assumption of our whole analysis is that $\nu a\ll 1$, so the F_n of (41) are always much smaller in magnitude than $c/(4\pi)$.

In Fig. 2 we show how the transmission of light of different polarizations is affected by the grating parameters t/a and ρ_h/ρ_l. For all the curves we held fixed $\nu a=0.005$ and $\rho_h=1000\ \Omega$. The polarizing property of the grating quickly becomes evident as ρ_h/ρ_l increases with T_z falling to zero (eventually as ρ_l^2) and T_y saturating. The saturation value of T_y decreases with decreasing t/a because the width of the highly conducting strips is thereby increased. The choice of $\rho_h=1000\ \Omega$ can be viewed as a compromise between two opposing behaviors. A larger ρ_h gives a larger saturation value of T_y, but one would need then to make the ratio ρ_l/ρ_h smaller to get the same amount of polarizing effect. In the other direction, a smaller ρ_h decreases the saturation value of T_y but increases the polarizing action as ρ_h/ρ_l increases. Typically experimental values have

$$\rho_h>\frac{4\pi}{c}=377\ \Omega>\rho_l \ . \tag{42}$$

For all the results plotted in Fig. 2 we used (32) and (34) and cut off the cosine Fourier sums at $n=10$, which sets the size of the matrix to be inverted in solving (34). We checked for various cases that the results are not sensitive to this choice. In contrast, we could not find a satisfactory result for the solution of (22) plus (27) once ρ_h/ρ_l exceeded ten. Hence for all the figures we only show results that use Eq. (32), rather than (26), to evaluate j_0. The upper limit on the Fourier sums will be held at 10.

Now include the 2D-EG. Its response is here de-

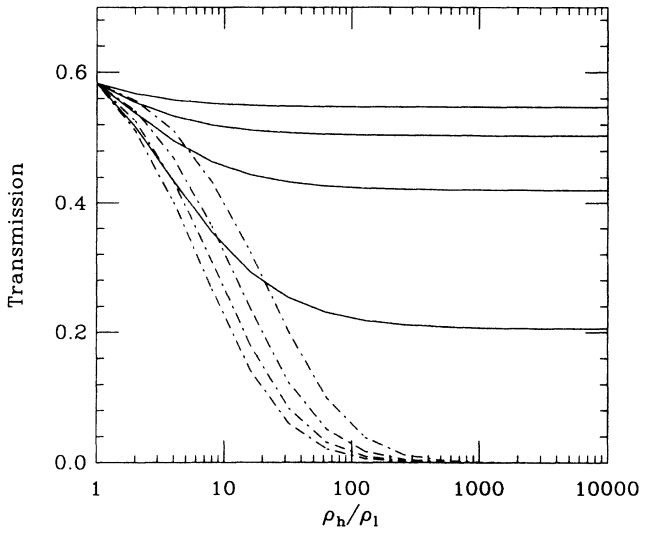

FIG. 2. Transmission coefficients through an interface that has a planar grating but no 2D-EG. The substrate has $\epsilon_s=12.8$ and the grating parameters t/a and ρ_h/ρ_l are varied with νa and ρ_h fixed. The solid (dashed) curves are for light polarized across (along) the grating strips. Four choices of t/a are illustrated: $t/a=0.7,0.5,0.3,0.1$, and the transmission coefficient for each polarization decreases monotonically with decreasing t/a.

scribed by the surface conductivity

$$\underline{\sigma} = \begin{bmatrix} \sigma & \sigma' \\ -\sigma' & \sigma \end{bmatrix} \tag{43}$$

whose elements are

$$\sigma = \tfrac{1}{2}(\sigma_+ + \sigma_-) ,$$
$$\sigma' = \tfrac{1}{2} i(\sigma_+ - \sigma_-) , \tag{44}$$

where

$$\sigma_\pm = \frac{Ne^2\tau}{m^*} / [1 - i(\omega_\pm \omega_c)\tau] \tag{45}$$

and

$$\omega_c = |e| B_0 / m^* c \tag{46}$$

with B_0 the static magnetic field pointing along $\hat{\mathbf{x}}$. As noted earlier, these semiclassical results have no wave-vector dependence so $\underline{\sigma}$ only shows significant structure near the cyclotron frequency ω_c, and not near harmonics.

In Fig. 3 we plot the fractional change in transmission of an unpolarized incident wave near the cyclotron resonance. The ordinate is

$$\Delta T/T = [T(B_0 = 0) - T(B_0)]/T(B_0 = 0) \tag{47}$$

and the material parameters have been chosen to model the data in Ref. 9. Consistent with experiment, the grating significantly increases the strength of the resonance (to above 50%) and slightly reduces its width. Across the center of the resonance j_0/e_y is less than $(900\ \Omega)^{-1}$ in magnitude, while the constant $\bar{\sigma} \approx (2\ \Omega)^{-1}$. Hence in view of Eq. (35) it is not surprising that the "perfect polarizer" approximation yields essentially the same results for $\Delta T/T$ as the full grating calculation.

The grating results are fairly sensitive to the value of τ, as shown in the inset of Fig. 3. [For this system the mobility μ is related to τ by $\tau(\text{psec}) = 40.4\mu(10^6\ \text{cm}^2\text{V}^{-1}\text{s}^{-1})$.] The results for no grating remain below 50%, while those with the grating can increase up to 100%. The choice $\tau = 5.5$ psec, holding all other parameters fixed, gives a maximum to $\Delta T/T$ that matches the 58% reported in Ref. 9. There is less sensitivity to small changes in the grating parameters; but this qualitative remark only holds for the cyclotron resonance region, where the primary influence of the grating is its action as a linear polarizer.

This last point is illustrated in Fig. 4, where we plot $\Delta T/T$ over a wider frequency range. Essentially the same parameters are used as in Fig. 3, but the effect of different choices of t/a is shown. Contrast in particular the significant changes in the strength of the first two magnetoplasmon resonances, near 77.2 and 92.7 cm^{-1}, against the nearly constant shape of the cyclotron resonance peak. A similar behavior occurs if we vary ρ_h/ρ_l; specifically as $\rho_h/\rho_l \to 1$ all the magnetoplasmon peaks disappear while the cyclotron resonance peak merely drops below 50%. In all of these variations the peak positions do not noticeably shift. For the magnetoplasmons the peak locations are well described by the zeros in the real part of the denominator of the F_n, which for $\omega_c\tau \ll 1$

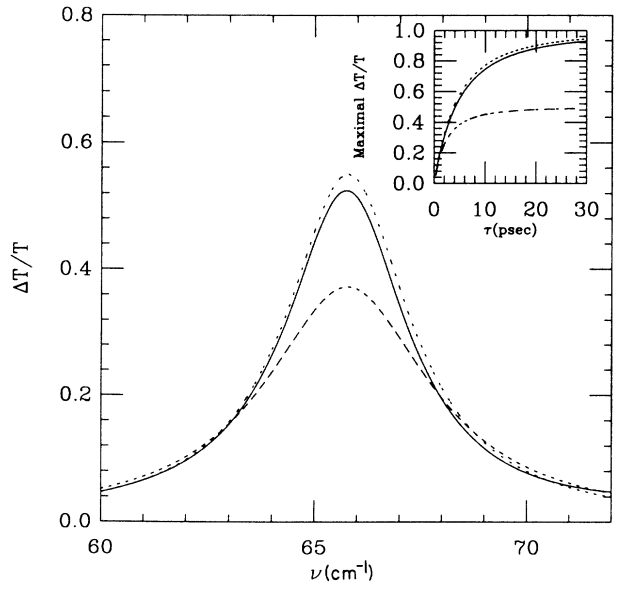

FIG. 3. Fractional change in transmission, Eq. (46), due to cyclotron resonance. Results both without (long dashes) and with (solid) a grating present are shown. The 2D-EG has $N = 6.7 \times 10^{11}/\text{cm}^2$, $m^*/m = 0.071$, and $\tau = 4.5$ psec; its cyclotron resonance in the B field of 5 T is at $\nu_c = 65.6\ \text{cm}^{-1}$. Referring to Fig. 1 we use for the substrate $\epsilon_0 = \epsilon_s = 12.8$ and for the grating $a = 0.872\mu m$, $d = 800$ Å, $t/a = 0.5$, $\sigma_h = 1/(1\ \Omega)$, and $\sigma_l = 1/(2000\ \Omega)$. The short-dashed curve is from the "perfect polarizer" expression in (2). In the inset we show the variation with τ of the maximum value of $\Delta T/T$ at ν_c.

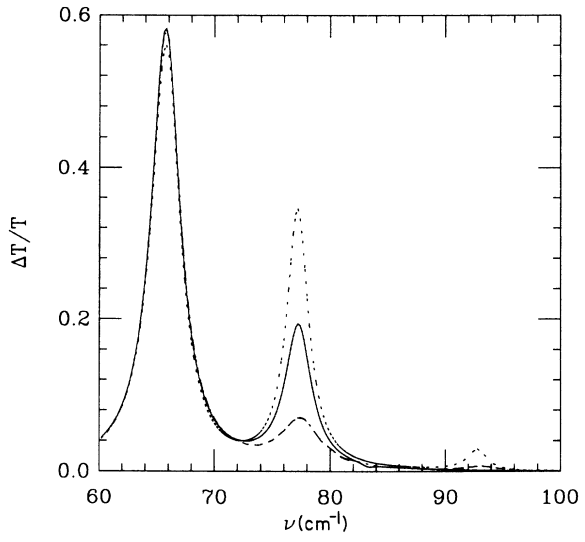

FIG. 4. Fractional change in transmission, Eq. (46), due to both cyclotron and magnetoplasmon resonances. The same parameters are used as in Fig. 3, except that $\tau = 5.5$ psec here and that calculations for three different corrugations are shown. The results plotted as solid, dashed, and dotted curves are for t/a values of 0.5, 0.65, and 0.35, respectively.

may be expressed as

$$\omega_n^2=\omega_c^2+4\pi\frac{Ne^2}{m^*}G_n[\epsilon_s+\epsilon_0\coth(G_nd)]^{-1}\ ; \qquad (48)$$

i.e., the standard nonretarded dispersion for magnetoplasmons in a 2D-EG separated by d from a perfectly conducting gate. It is remarkable that this simple equation describes so well the peak locations in $\Delta T/T$.[20]

At a qualitative level, all of the remarks made in the last paragraph have been known since the perturbation expressions were obtained.[4–8] In particular the sum of contributions in (37) describes approximately the influence of the grating on excitations at wave vectors G_k. The factor of $\tilde{\rho}^2(k)$ contains the strong t/a and ρ_h/ρ_l dependence of the magnetoplasmon peaks—see (40)—and the F_k determines the peak locations. However, Eq. (37) is not always quantitatively reliable, as we show in Fig. 5, which is based on the parameters of Ref. 4. In Fig. 5(a) we use the value of τ reported in the experiment and show $\Delta T/T$ calculated both from our complete theory and from the expansion (37) with no further approximation. The two theoretical estimates agree well with each other and with experiment.[4] Then in Fig. 5(b) we artificially increase τ by a factor of 10 and again compare the exact and perturbative predictions for $\Delta T/T$. There is now a significant disagreement between the two. The quantitative failure of the perturbation expansions is similar for the results shown in Fig. 4; the perturbative magnetoplasmon amplitudes there are off by about a factor of 2. Since τ in the samples available nowadays is still larger,[21] our nonperturbative approach should find many future applications.

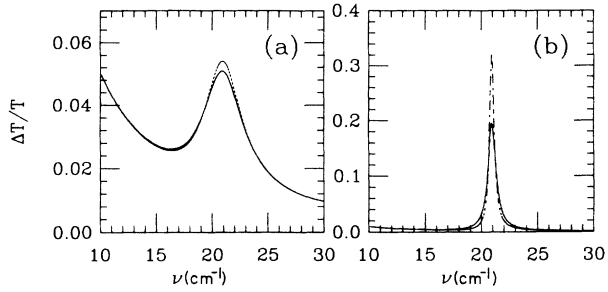

FIG. 5. Fractional change in transmission due to the presence of a 2D-EG. Both the exact (solid) and perturbative (dashed) results are shown. The 2D-EG has $N=1.55\times10^{12}/\text{cm}^2$ and $m^*/m=0.2$. There is no static B field. Referring to Fig. 1 we use $\epsilon_0=4$, $\epsilon_s=12$, and for the grating $a=3.52$ μm, $d=1400$ Å, $t/a=0.65$, $\sigma_h=1/(0.1\ \Omega)$, and $\sigma_l=1/(350\ \Omega)$. In panel (a) $\tau=1.35$ psec, while in panel (b) $\tau=13.5$ psec.

ACKNOWLEDGMENTS

We wish to thank Professor J. P. Kotthaus for suggesting this problem, and Dr. D. Heitmann and Dr. E. Batke for helpful discussions of experimental details. We are especially grateful to Dr. D. Heitmann for providing a copy of the Ph.D. thesis of Dr. T. N. Theis. Our work was supported in part by the National Science Foundation through Grants No. DMR-85-12709 and No. DMR-88-02383. Some of the computations were done on the Cray Research, Inc. X-MP/48 system at the National Center for Supercomputing Applications at the University of Illinois at Urbana-Champaign (Champaign, IL).

[1]D. Heitmann, Surf. Sci. **170**, 332 (1986).
[2]J. P. Kotthaus, in *Interfaces, Quantum Wells, and Superlattices,* edited by C. R. Leavens and R. Taylor (Plenum, New York, 1988), p. 95.
[3]D. Heitmann, in *Physics and Applications of Quantum Wells, and Superlattices,* edited by K. v. Klitzing and E. E. Mendez (Plenum, New York, 1988), p. 317.
[4]S. J. Allen, Jr., D. C. Tsui, and R. A. Logan, Phys. Rev. Lett. **38**, 980 (1977).
[5]T. N. Theis, Surf. Sci. **98**, 515 (1980).
[6]D. C. Tsui, S. J. Allen, Jr., R. A. Logan, A. Kamgar, and S. N. Coppersmith, Surf. Sci. **73**, 419 (1978).
[7]T. N. Theis, J. P. Kotthaus, and P. J. Stiles, Solid State Commun. **24**, 273 (1977).
[8]T. N. Theis, J. P. Kotthaus, and P. J. Stiles, Solid State Commun. **26**, 603 (1978).
[9]E. Batke, D. Heitmann, and C. W. Tu, Phys. Rev. B **34**, 6951 (1986).
[10]D. Heitmann, J. P. Kotthaus, U. Mackens, and W. Beinvogl, Superlatt. Microstruct. **1**, 35 (1985).
[11]U. Mackens, D. Heitmann, L. Prager, J. P. Kotthaus, and W. Beinvogl, Phys. Rev. Lett. **53**, 1485 (1984).
[12]J. P. Kotthaus, W. Hansen, H. Pohlmann, M. Wassermeier, and K. Ploog, Surf. Sci. **196**, 600 (1988).
[13]F. Brinkop, W. Hansen, J. P. Kotthaus, and K. Ploog. Phys. Rev. B **37**, 6547 (1988).
[14]*Electromagnetic Theory of Gratings,* edited by R. Petit (Springer, New York, 1980).
[15]P. Park, A. H. MacDonald, and W. L. Schaich (unpublished).
[16]E. Batke, D. Heitmann, J. P. Kotthaus, and K. Ploog, Phys. Rev. Lett. **54**, 2367 (1984).
[17]A. V. Chaplik and D. Heitmann, J. Phys. C **18**, 3357 (1985).
[18]W. L. Mochan and R. G. Barrera, Phys. Rev. B **32**, 4984 (1985).
[19]T. N. Theis, Ph.D. thesis, Brown University.
[20]An exception to this claim occurs if the grating has regions of very large resistivity. The usual practive of having a uniform layer of NiCr with $\rho\sim10^3\ \Omega/\square$ removes this difficulty.
[21]M. Tewordt, E. Batke, J. P. Kotthaus, G. Weimann, and W. Schlapp. in *Proceedings of the International Conference on the Applications of High Magnetic Fields in Semiconductor Physics, Würzburg, 1988,* edited by G. Landwehr (Springer, Berlin, 1989).